Kinetics of Electron Transfer at Pt Nanostructured Film Electrodes

Sarah L. Horswell, Ian A. O'Neil, and David J. Schiffrin*

Centre for Nanoscale Science, Department of Chemistry, University of Liverpool, Liverpool L69 7DZ, UK

Received: January 6, 2003; In Final Form: March 20, 2003

The kinetics of electron transfer to nanoparticulate platinum/octyldiisocyanide films has been investigated. The films were grown by attachment of 1,8-diisocyanooctane onto gold, and Pt layers were constructed by contacting this film with a toluene solution of Pt nanoparticles. Repeating this procedure gave multilayer films. The rate of electron exchange between these and the hexacyanoferrate redox couple was investigated using three different techniques: cyclic voltammetry, rotating disk electrode, and ac impedance. For isocyanide-terminated films, incomplete coverage by the ligand resulted in a behavior similar to that of a partially blocked electrode. Good electronic communication throughout the film was apparent when the surface contained attached Pt nanoparticles. The measured rate constant decreased with increasing number of layers, and this effect has been ascribed to a reduced number of active sites where electron transfer can take place. The self-assembly method used is of interest for the self-organization of transition metal nanoparticles at electrode surfaces.

1. Introduction

The practical development of fuel cells for traction applications has required an understanding of the structure and properties of the platinum group metal nanoparticles used as electrocatalysts. In particular, a central outstanding issue is the relationship between size and reactivity.[1] An example of how the dimensions of clusters can determine their chemical behavior is the remarkable change in reactivity of gold toward CO oxidation. Bulk gold is a poor catalyst but Au nanoparticles show high activity. This is also the case for various hydrogenation reactions and the reduction of nitrogen oxides.[2] Importantly, even for core−shell nanoparticles, i.e., gold clusters capped with an alkane thiol layer, reactivity for the electrochemical oxidation of CO is clearly in evidence.[3]

There has been considerable interest in the preparation of nanoparticles for use as building blocks.[4] It is well recognized that these materials can be used in much the same way as chemical compounds in the construction of multilayer structures[5,6] that are of interest for the study of electron transfer between nanoparticles present in a film[5e,6a] or between the film and solution redox species.[5f] The attachment of well-characterized nanoparticles to electrode surfaces can be a powerful method to investigate reactivity. For example, the difference in the infrared spectra of CO adsorbed on bulk Pt and on Pt nanoparticles can help to probe their electrocatalytic properties.[7] Importantly, Murray et al. have demonstrated that quantum size effects can be observed with nanoparticles[6a,8] and that electrons confined in them[8d] can be made to enter electrochemical reactions in a controlled manner. Thus, monolayer-capped nanoparticles can represent a new state of matter between single redox molecules and bulk metals.

Most of the work on the electrochemical properties of arrays of nanoparticles has been carried out with coinage metals. To investigate catalytic materials such as Pt, appropriate tethers for attachment are required. Due to their versatility for coordination to transition metal surfaces, isocyanides have been employed as ligands.[9]

Pt has been used in the present work due to the applications of this metal in electrocatalysis. Pt nanoparticle solutions are easily prepared by the reduction of Pt salts with a variety of reducing agents,[10] and size and shape can be controlled by the choice of the reaction conditions.[10f,11,12] A great variety of stabilizing agents has been used to prevent particle aggregation including strongly adsorbed molecules,[13] polymers and surfactants,[10a,g,14] and tetraalkylammonium salts.[12,15] The advantage of the latter is the stability of these preparations which are, at the same time, sufficiently reactive to allow further reaction of the metal with other ligands. This can be exploited to self-assemble particles onto surfaces bearing functional binding groups.[5a,c−h,9b,16]

The purpose of the present work was to study electron transfer across mono- and multilayers of Pt nanoparticles attached to a gold substrate using a bifunctional isocyanide linker. It was of particular interest to ascertain if the kinetics of electron transfer between the nanostructured film and the aqueous hexacyanoferrate (II)/(III) couple was affected by the surface termination. The values of the measured rate constants can be dependent on the measuring method employed, and for this reason a comprehensive study employing three different techniques was undertaken.

2. Experimental Details

The techniques employed for the measurement of rate constants were cyclic voltammetry (CV), the rotating disk electrode (RDE), and ac impedance spectroscopy. The electrodes were prepared as follows. Au disk electrodes were first treated with a concentrated nitric acid and sulfuric acid mixture to ensure removal of adsorbed isocyanide from previous experiments. These were then polished with suspensions of successively finer grades of alumina powder (1, 0.3, and 0.05 μm, Buehler), rinsed, and placed in pure water in an ultrasonic bath for several minutes. Prior to electrochemical measurements, electrodes were cycled in deoxygenated base electrolyte between the onset potentials of hydrogen and oxygen evolution to further clean the surface and to ensure reproducibility.[17] The electrolyte was then discarded and a fresh solution was used for the experiments. The nanostructures studied were prepared using

* Corresponding author. E-mail: d.j.schiffrin@liv.ac.uk.

10.1021/jp0340257 CCC: $25.00
Published on Web 04/25/2003

1,8-diisocyanooctane (DICO) as the ligand and a toluene solution of Pt nanoparticles stabilized by quaternary ammonium salts. Their syntheses have been described elsewhere.[9]

The electrodes were first derivatized by immersion in a toluene (Fluka, puriss) solution of 1,8-diisocyanooctane for 18 h,[9b] and after thoroughly rinsing with toluene, they were subsequently derivatized with Pt nanoparticles by immersion in the toluene solution of Pt nanoparticles for 18 h. Further layers were built up by repeating this procedure using, alternately, diisocyanide and Pt nanoparticle solutions. Immediately prior to use, derivatized electrodes were rinsed with toluene, dried in a stream of nitrogen, and rinsed with water.

Water was purified in a Millipore system. K_2SO_4 (BDH, AnalaR) and $K_4Fe(CN)_6$ (BDH, AnalaR) were used as received. The glassware was cleaned with a 1:1 mixture of concentrated nitric and sulfuric acids followed by rinsing with pure water.

Cyclic voltammetry experiments were conducted in a standard three-electrode cell of 0.02 dm^3 volume. The counter electrode was a Pt gauze cleaned by flame annealing, and the reference electrode was a saturated calomel electrode (SCE). All potentials are quoted with respect to this electrode. For the cyclic voltammetry experiments, the Pt working electrode was a Pt wire (99.998%, Johnson Matthey) sealed in borosilicate glass, area 0.316 cm^2, which was cleaned by flame annealing before use. The Au electrode was made of an Au wire (99.998%, Johnson Matthey) sealed in soda glass to expose a disk of 0.0154 cm^2 area. All experiments were conducted in 1 mM $K_4Fe(CN)_6$ + 0.1 M K_2SO_4. OFN nitrogen (BOC Gases) was used to eliminate oxygen from the solution.

The potential was controlled with an Autolab PGStat 20 system (EcoChemie, The Netherlands), but for the impedance measurements, a Hi-Tek DT11001 potentiostat controlled by a Hi-Tek PPR1 waveform generator was used. The half-wave potential was determined from the RDE results. The ac impedance measurements were carried out with a Solartron 1250 frequency response analyzer controlled by Solartron software.[18] The bias potential was set by the waveform generator and potentiostat, and measurements were taken at several potentials at either side of the formal potential in order to check the reliability of the measurements. The signal amplitude was 10 mV, and the frequency range employed was 0.1 to 10000 Hz, averaging over 3 cycles for each frequency. The ac impedance experiments were carried out in the same cell used for cyclic voltammetry. Baseline measurements were also conducted in 0.1 M K_2SO_4 in the absence of the redox couple, and the results were analyzed on a PC.[18]

Rotating disk measurements were conducted in a three-electrode cell of 0.1 dm^3 volume. As for the cyclic voltammetry experiments, the counter and reference electrodes were a Pt gauze and an SCE, respectively. The SCE was situated in a separate compartment with a Luggin capillary tip. The working electrodes were Au (area 0.0707 cm^2) and Pt (area 0.196 cm^2) sealed in PTFE and mounted on the shaft of the disk support (ED/101, Radiometer, Copenhagen). The rotation rate was controlled with a CVT101 speed control unit (Radiometer, Copenhagen). The solutions were deaereated with nitrogen, and a stream of nitrogen was maintained over the solution during measurements. Polarization curves were recorded at a scan rate of 2 mV s^{-1} at different rotation rates.

3. Measuring Techniques

The rate constants were measured by three different techniques: cyclic voltammetry, the rotating disk electrode (RDE), and ac impedance spectroscopy. For a general quasi-reversible reaction, $O + ne^- = R$, the electrochemical rate constant can be calculated from the peak separation dimensionless parameter ψ given by[19,20]

$$\psi = \frac{\left(\frac{D_O}{D_R}\right)^{\alpha/2} k^{0'}}{\sqrt{D_O \pi \upsilon nF/RT}} \quad (1)$$

where D_O and D_R are the diffusion coefficients of the oxidized and reduced species, respectively, α is the transfer coefficient, $k^{0'}$ is the formal rate constant in cm s^{-1}, and υ is the sweep rate. A value of $\alpha = 0.5$ was assumed throughout. ψ was calculated at each sweep rate from the peak potential separation,[19,20] and $k^{0'}$ was calculated from the linear regression of the dependence of ψ on $\nu^{-1/2}$ (eq 1). The ratio D_R/D_O was taken as 0.68.[21]

For a quasi-reversible reaction at a RDE, the dependence of the current density on rotation rate is given by[19]

$$\frac{1}{j} = \frac{1}{nF(k_b c_R^* - k_f c_O^*)}\left[1 + \frac{{D_O}^{-2/3} k_f + {D_R}^{-2/3} k_b}{0.62 \nu^{-1/6} \omega^{1/2}}\right] \quad (2)$$

Here, k_f and k_b are the forward (oxidation) and backward (reduction) rate constants, respectively, at a given potential, c_O^* and c_R^* are the bulk concentrations of the oxidized and reduced components of the redox couple, ν is the kinematic viscosity, and ω is the rotation rate in rad s^{-1}. The rate constants are given by

$$k_f(E) = k^{0'} \exp[-\alpha f(E - E^{0'})] \quad (3)$$

and

$$k_b(E) = k^{0'} \exp[(1 - \alpha) f (E - E^{0'})] \quad (4)$$

where $f = F/RT$; $E^{0'}$ is the formal potential of the electrochemical reaction, and α refers to the reduction reaction. Equations 2, 3, and 4 were used to evaluate the electron-transfer rate constants.

The ac impedance spectroscopy results were analyzed using the Randles equivalent circuit.[19] Briefly, the interfacial impedance components are calculated as a series combination of a resistance R_s and a pseudo capacitance C_s after correction for the solution resistance and double-layer capacitance. This was achieved by subtracting the real and imaginary components of the base electrolyte admittance from the corresponding components of the admittance in the presence of the redox couple, using the admittances of the base electrolyte and of the solution being measured. R_s is the sum of the charge-transfer resistance, R_{CT}, and the real part of the Warburg impedance. C_s is the imaginary component of the Warburg impedance.

These quantities are related to the frequency of the applied ac signal through

$$R_s = R_{CT} + \sigma/\omega^{1/2} \quad (5)$$

$$C_s = 1/\sigma\omega^{1/2} \quad (6)$$

where ω is the angular frequency and

$$\sigma = \frac{1}{n^2F^2\sqrt{2}}\left(\frac{1}{c_O^* D_O^{1/2}} + \frac{1}{c_R^* D_R^{1/2}}\right) \quad (7)$$

Therefore,

$$R_{CT} = R_s - 1/\omega C_s \quad (8)$$

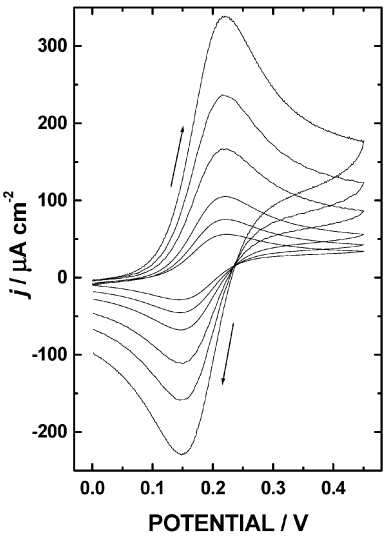

Figure 1. Cyclic voltammetry for the oxidation of ferricyanide on a Au electrode. Sweep rates for increasing peak currents: 5, 10, 20, 50, 100, and 200 mVs^{-1}. The solution contained 1 mM $K_4Fe(CN)_6$ + 0.1 M K_2SO_4.

There are two methods for calculating kinetic parameters from impedance measurements. In the first, originally used by Randles, the real and imaginary components of the base electrolyte corrected impedance (R_s and $1/\omega C_s$) are plotted against $\omega^{-1/2}$. The plots are linear and of equal slope σ, and the plot of the imaginary component should pass through the origin. The difference between the intercepts gives the value of the charge-transfer resistance. From this, the standard rate constant can be calculated from

$$k^{0\prime} = \frac{j_0}{nFc_O^{1-\alpha}c_R^{\alpha}} = \frac{RT}{n^2F^2c_O^{1-\alpha}c_R^{\alpha}R_{CT}} \quad (9)$$

where j_0 is the exchange current density. The concentrations of the oxidized and reduced species are equal to half of the bulk concentration of hexacyanoferrate (II) at the formal potential. R_{CT} was also calculated by nonlinear regression analysis of the impedance spectra.[18,19]

4. Results

The oxidation of hexacyanoferrate(II) has been used throughout this work to probe the influence of the Pt nanostructures on the rate of electron transfer. Figure 1 shows the cyclic voltammetry of hexacyanoferrate(II) on a bare Au electrode, where the characteristic reversible behavior of this system can be observed. Figures 2a−d compare the same reaction for this electrode with an attached monolayer of DICO, (a), and for electrode surfaces functionalized with layers of DICO/Pt, (b), DICO/Pt/DICO, (c), and DICO/Pt/DICO/Pt, (d). Pt indicates in this case a layer of attached Pt nanoparticles. These results show that the voltammetric behavior is strongly influenced by the surface termination. When the surface is terminated with diisocyanide the response resembles that of a microelectrode array, whereas a voltammetric behavior characteristic of a quasi-reversible reaction on a planar electrode is observed when the surface is terminated with metal nanoparticles. The currents observed for isocyanide-terminated surfaces were always much smaller than those for Pt-terminated layers (compare Figures 2a and 2c with 2b and 2d, respectively). The peak currents observed decreased with increasing number of layers. For example, a decrease of approximately 40% was observed between electrodes with one and three isocyanide−Pt layers (data not shown).

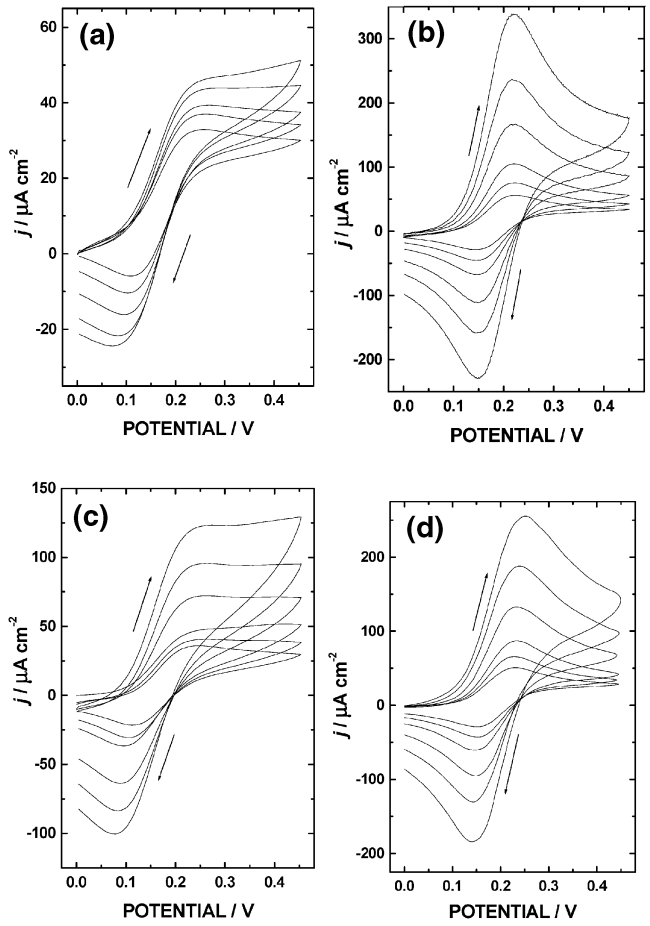

Figure 2. Experimental conditions the same as in Figure 1, but for electrodes derivatized with (a) 1,8-diisocyanooctane (DICO); (b) DICO + a monolayer of Pt nanoparticles (DICO | Pt); (c) a further layer of DICO attached to the Pt nanoparticles (DICO | Pt | DICO); and (d) the previous surface terminated with Pt nanoparticles (DICO | Pt | DICO | Pt).

Figure 3 shows a comparison of the polarization curves obtained on a rotating disk electrode for (a) bare gold, (b) Au functionalized with DICO, and (c) the latter after attachment of Pt nanoparticles. Similarly to the cyclic voltammetry results described above, a diisocyanide termination does not lead to complete inhibition of electron transfer but rather to a decrease in the limiting diffusional current by approximately a factor of 4. Attachment of Pt nanoparticles to the film resulted in restoration of electrode activity, but the limiting diffusional current was smaller than that for bare gold. The limiting current decreased with an increase in the number of layers, as can be seen in Figure 4. A decrease of approximately 30% between one and three Pt layers was observed.

Similar trends as discussed above can be observed from the ac impedance results. Figure 5a shows the impedance for a bare Au electrode, and Figure 5b shows the results when a single monolayer of isocyanide is attached to the surface. The spectrum displays a semicircle characteristic of an irreversible charge-transfer reaction coupled to a more complex behavior at low frequencies. Figure 5c shows the same plot when Pt nanoparticles are attached to the ligand layer and a large increase in rate constant is apparent. Figure 5d shows the spectrum of a three-layer structure with a Pt nanoparticle termination. (The data for the intermediate DICO-terminated electrode are not shown.) It is noteworthy that the slope of the dependence of

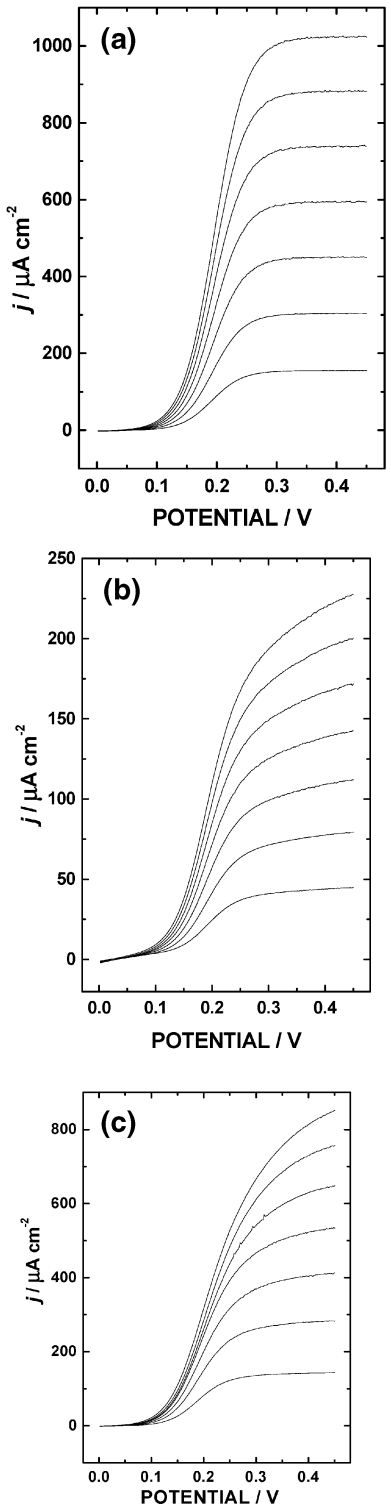

Figure 3. Current−potential curves for a rotating disk electrode in contact with 1 mM $K_4(CN)_6$ + 0.1 M K_2SO_4: (a) Au; (b) Au | DICO; (c) Au | DICO | Pt. The rotation rates for increasing currents were 100, 400, 900, 1600, 2500, 3600, and 4900 rpm. The potential sweep rate was 2 mVs^{-1}.

the imaginary component, Z'', on the real part, Z', changes from 45° to 22.5° as the thickness of the film increases. The latter dependence is characteristic of porous materials.[22]

5. Rate Constant Calculations

5.1. Cyclic Voltammetry. The rate constants for Pt-terminated surfaces were calculated from the sweep rate dependence of ψ (eq 1); the corresponding plots are shown in Figure 6 and the calculated values of the rate constants are shown in Table 1. This analysis could not be carried out for the DICO-terminated electrode layers since the voltammetric behavior was inconsistent with that expected for an electrode displaying linear diffusion behavior (see below).

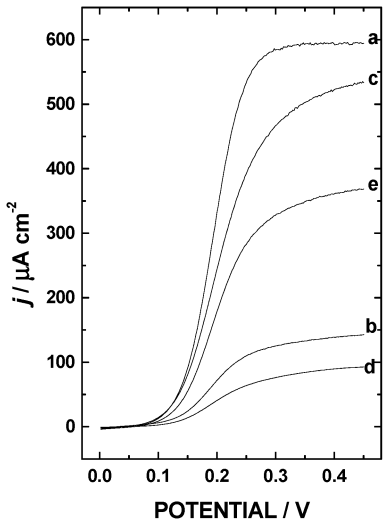

Figure 4. Comparison of current−potential curves at 1600 rpm (see Figure 3) for different surface terminations: (a) bare gold; (b) gold with one layer of DICO; (c) DICO | Pt; (d) DICO | Pt | DICO | Pt | DICO; and (e) DICO | Pt | DICO | Pt | DICO | Pt.

TABLE 1: Rate Constants for Electron Transfer for Pt-Terminated Electrodes from Cyclic Voltammetry

electrode	$10^3 \times k^{0\prime}$/cm s^{-1}
Au	41 ± 30
Au | DICO | Pt	4.2 ± 0.1
Au | DICO | Pt | DICO | Pt	5.7 ± 0.3
Au | DICO | Pt | DICO | Pt | DICO | Pt	2.1 ± 0.3

5.2. Rotating Disk Electrode. These results were analyzed using two different methods, Koutecky−Levich (K.−L.) plots and nonlinear regression analysis. Figure 7 shows some typical K.−L. plots obtained. The strong potential dependence of the slope is related to the quasi-equilibrium conditions prevailing at the electrode surface. From eqs 2, 3, and 4, it is easy to show that

$$j^{-1} = \frac{1}{Fc_R^* k^{0\prime} \exp^{(1-\alpha) f(E-E^{0\prime})}} + \frac{1 + b \exp^{-f(E-E^{0\prime})}}{0.62 D_R^{2/3} F c_R^* \nu^{-1/6} \omega^{1/2}} \quad (10)$$

where c_R is the bulk concentration of the electroactive species and b is given by

$$b = \left(\frac{D_R}{D_O}\right)^{2/3} \quad (11)$$

Therefore, the K.−L. slope ($S(E)$) is

$$S(E) = \frac{1 + b \exp^{-f(E-E^{0\prime})}}{0.62 D_R^{2/3} F c_R^* \nu^{-1/6}} \quad (12)$$

From eqs 10, 11, and 12, the potential dependence of the K.−L. slope can be conveniently expressed as

$$E = E^{0\prime} - \frac{2.303RT}{F}\left[\log\left(\frac{D_O}{D_R}\right)^{2/3} + \log\left(\frac{S(E)}{S_{lim}} - 1\right)\right] \quad (13)$$

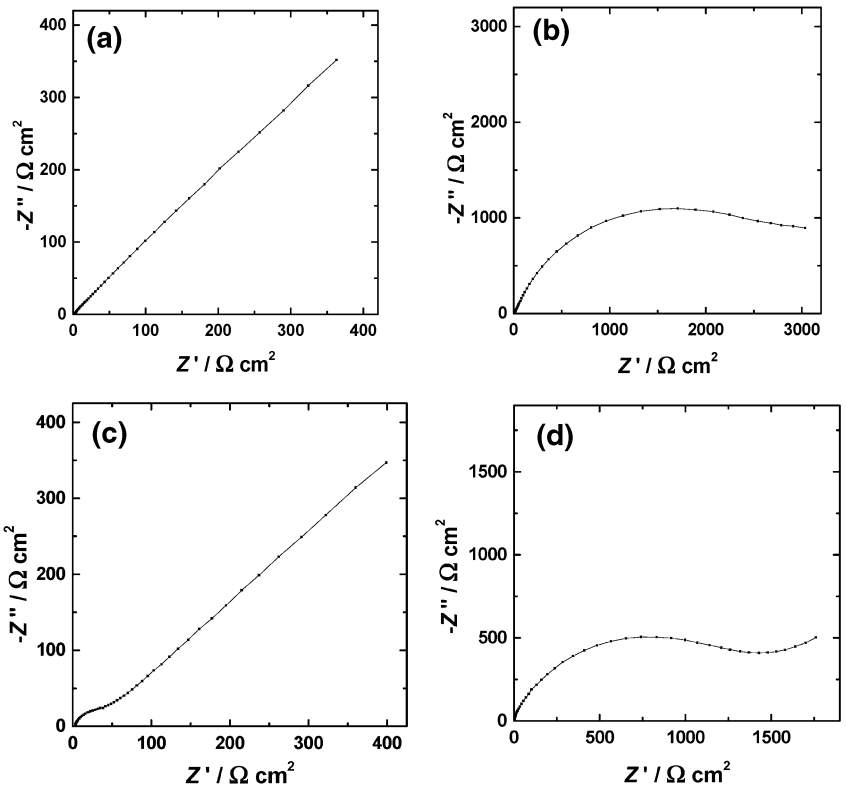

Figure 5. Complex ac impedance plots for Au electrodes with various surface terminations in contact with 1 mM $K_4Fe(CN)_6$ + 0.1 M K_2SO_4: (a) Au; (b) one layer of 1,8-diisocyanooctane; (c) Au | DICO | Pt; and (d) Au | DICO | Pt | DICO | PT | DICO | Pt. The potential was set at 0.195 V (the measured formal potential of the hexacyanoferrate(II)/(III) couple) and using a 10 mV peak to peak potential modulation. The frequency range was 0.1−5000 Hz.

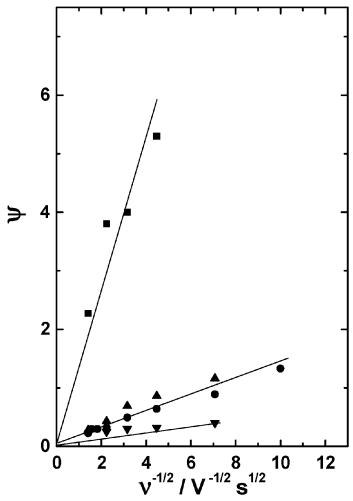

Figure 6. Dependence of the parameter ψ (see eq 1) on sweep rate for different Pt nanoparticle-terminated electrode surfaces. Data from cyclic voltammetry: ■ bare gold; ● DICO | Pt; ▲ DICO | Pt | DICO | Pt, and ▼ DICO | Pt | DICO | Pt | DICO | Pt.

where S_{lim} is the limiting value of the K.−L. slope at very positive potentials. Figure 8 shows a test of this relationship. The slope of this plot is 61.5 mV decade^{-1}, which compares well with the theoretical value of 59.2 mV decade^{-1}showing that the analysis for a quasi-reversible reaction is appropriate for the present results.

Values of the formal rate constants were calculated from eq 10, from the K.-L. intercepts and an example of the potential dependence of the limiting currents obtained for $\omega \rightarrow \infty$ is shown in Figure 9. Some curvature in these Tafel plots was apparent for all the electrode surfaces investigated. This behavior has been previously observed[23] and its origin is unclear; it could result from a potential dependent charge-transfer coefficient,[23] from surface blocking effects,[24] or from the reliance on extensive extrapolations as required for the calculation of kinetic currents from K.−L. plots. A better approach is to obtain kinetic information directly by the nonlinear regression (NLR, Microcal Origin software, version 6.0) fitting to eq 10 of the full polarization curves at different rotation rates. This technique has recently been employed successfully to deconvolute the more complex case of a 2-site electrocatalytic oxygen reduction[25] and is advantageous in providing objective criteria for calculating reaction parameters and for the error analysis of the values obtained. A typical example of such fittings is shown in Figure 10.

The results obtained by NLR of the RDE data for all the electrodes investigated and the corresponding standard deviations are shown in Table 2. For a given electrode surface, the fitting procedure was carried out for each rotation rate and the average value of the rate constant was then calculated. The formal potential of the hexacyanoferrate (II)/(III) couple was calculated by nonlinear regression of all the measurements for bare Pt and Au electrodes at different rotation rates, and a value of $E^{0'} = 0.195 \pm 0.002$ V was found. The value of α was fixed during the NLR procedure, and results for $\alpha = 0.5$ are given in this Table. The above calculations were repeated for different values of α and $k^{0'}$ changed by ±10% for a change of α of ±0.1. Thus, the value of α does not affect the observed trend in the values of the rate constants calculated compared with the error bands of the techniques employed. A value of $\alpha = 0.5$ was used for all the calculations. This value is also in agreement with the results shown in Figure 9. The ratio D_R/D_O used was the same as for the analysis of the cyclic voltammetry results.

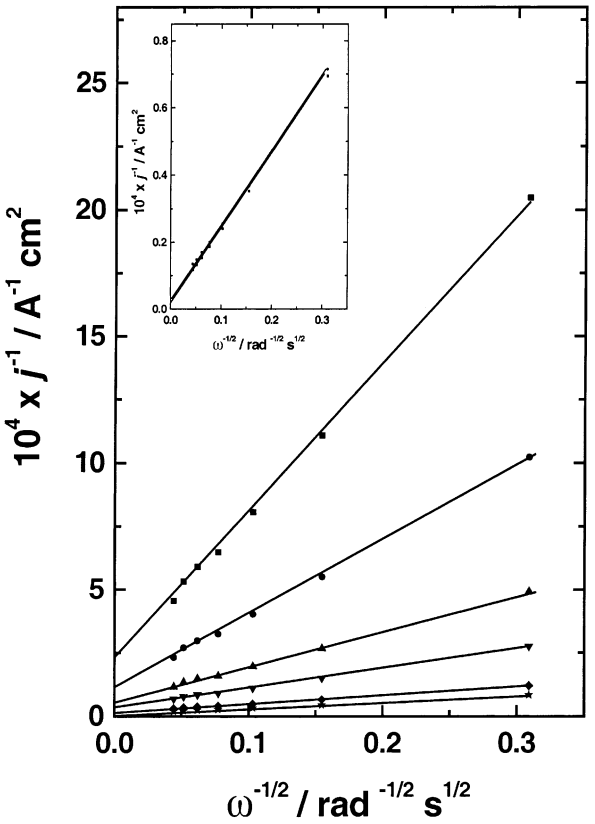

Figure 7. Koutecky−Levich plots for the oxidation of hexacyanoferrate(II) at different potentials for a Au | DICO | Pt electrode. Potentials: ■ 0.1 V; ● 0.12 V; ▲ 0.14 V; ▼ 0.16 V; ◆ 0.2 V; ★ 0.24 V. Inset: ■ 0.34 V; ● 0.45 V.

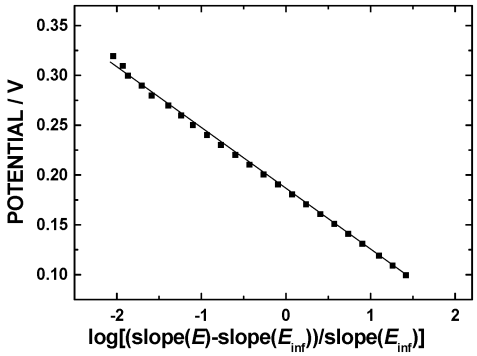

Figure 8. Analysis of the K.−L. slopes (Figure 7) based on eq 13 for a Au | DICO | Pt electrode in contact with 1 mM $K_4Fe(CN)_6$ + 0.1 M K_2SO_4.

5.3. AC Impedance. The ac impedance data for the bare Au and for the Au | DICO | Pt electrodes were analyzed using the Randles equivalent circuit.[19] This method is suitable only for electrodes with well-defined planar diffusional characteristics. The region of the ac impedance spectrum corresponding to diffusion control should yield a straight line at an angle of 45° on the impedance plot, and this was observed for these two electrodes (Figures 5a,c). The other electrode surfaces did not produce impedance spectra with these characteristics, probably due to the porosity of the attached layers. Therefore, the impedance spectra were analyzed using nonlinear regression fitting procedures that employ a parametric analysis of the diffusional component to the impedance.[18]

Figure 11 shows the dependence of R_s and C_s on $\omega^{-1/2}$ for the Au | DICO | Pt electrode, and R_{CT} was calculated from the difference between the intercepts of the two lines. Additionally,

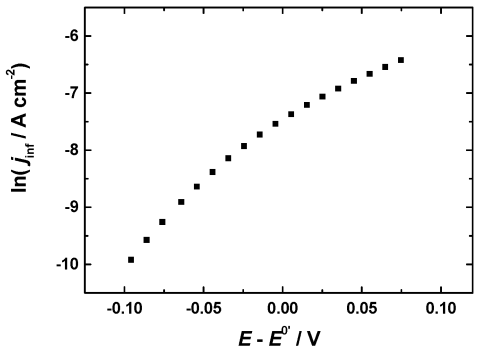

Figure 9. Tafel plot for the oxidation of hexacyanoferrate(II) for a Au | DICO | Pt electrode in contact with 1 mM $K_4Fe(CN)_6$ + 0.1 M K_2SO_4. The currents were calculated from the extrapolation of j^{-1} for $\omega \rightarrow \infty$ (eq 10).

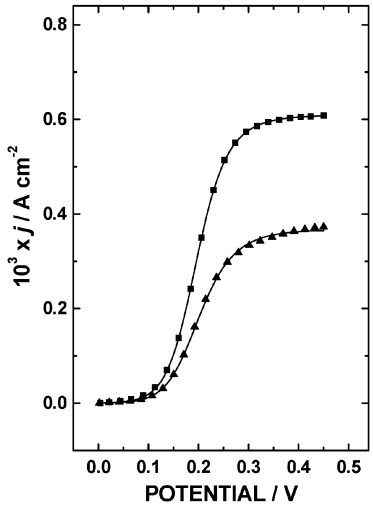

Figure 10. Examples of nonlinear regression fits for the rotating disk electrode results. ■ Bare Pt; ▲ Au | DICO | Pt | DICO | Pt | DICO | Pt. Both polarization curves were obtained at a rotation rate of 1600 rpm.

TABLE 2: Results of the Nonlinear Regression Analysis for the RDE Data[a]

electrode	$10^3 \times k^{0'}$/cm s^{-1} ($\alpha = 0.5$)
bare Au	20 ± 8
Au | DICO	2.5 ± 0.7
Au | DICO | Pt	6.0 ± 0.7
Au | DICO | Pt | DICO | Pt	3.9 ± 0.4
Au | DICO | Pt | DICO | Pt | DICO	1.1 ± 0.4
Au | DICO | Pt | DICO | Pt | DICO | Pt	4.9 ± 1
bare Pt	13 ± 5

[a] Standard deviations calculated for the data obtained for each of the 12 different rotation rates measured.

the Randles model assumes a negligible change in the electrolyte resistance and double layer capacitance when the redox couple is added to the solution. In all cases, the value of the double layer capacitance, C_{dl}, obtained from the fitting, increased when hexacyanoferrate(II) was present, and this may introduce some additional uncertainty in the calculations. Values of $k^{0'}$ of 0.055 ± 0.005 and 0.022 ± 0.002 cm s^{-1} were obtained for the Au and Au | DICO | Pt electrodes, respectively. These values compare well with those obtained with the nonlinear regression fit of the impedance data (see Table 3), considering the errors of these analysis techniques for fast reactions. For the latter, the charge-transfer resistance was measured at different potentials close to the formal potential.

TABLE 3: Rate Constants Calculated from the AC Impedance Data

electrode	$10^3 \times k^{0\prime}$/cm s^{-1} (from Randles equivalent circuit analysis)	$10^3 \times k^{0\prime}$/cm s^{-1} (from nonlinear regression of ac impedance spectra)[a]
Au	55 ± 5	78 ± 12
Au | DICO		0.19 ± 0.005
Au | DICO | Pt	22 ± 2	20.9 ± 0.6
Au | DICO | Pt | DICO		0.48 ± 0.005
Au | DICO | Pt | DICO | Pt		1.9 ± 0.1
Au | DICO | Pt | DICO | Pt | DICO | Pt		0.87 ± 0.05

[a] Standard deviations form the individual NLR fitting analysis.

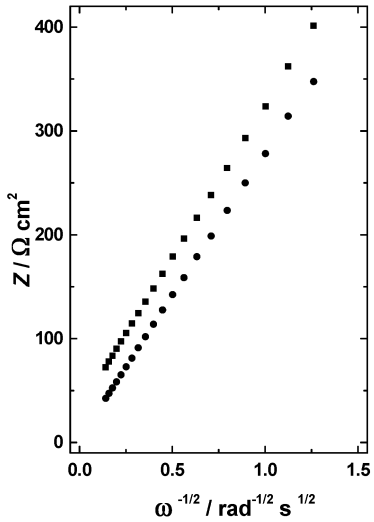

Figure 11. Impedance data analysis based on eqs 5−9 for a Au | DICO | Pt electrode in contact with 1 mM $K_4Fe(CN)_6$ + 0.1 M K_2SO_4. ■ R_s; ● $1/\omega C_s$.

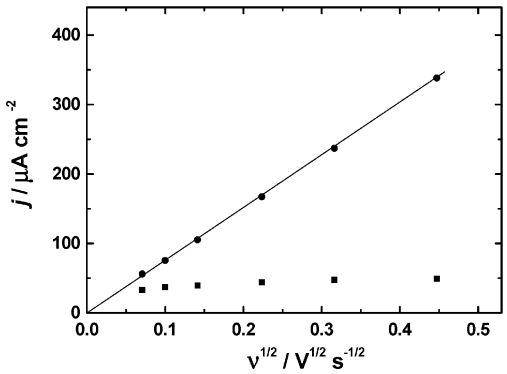

Figure 12. Comparison of peak current densities from CV results for a Au ● and a Au | DICO ■ electrode.

The rate constants obtained from the regression analysis are shown in Table 3. The Warburg impedance in the classical Randles circuit was changed for a constant phase element (CPE), and a CPE coefficient of 0.49 was obtained for a Au | DICO | Pt electrode, close to the value of 0.5 for a classical Warburg impedance. The regression analysis for the multilayer films was more difficult to carry out. Although the impedance plane plots gave an angle approaching 22.5° to the real axis at the low frequency limit, a CPE coefficient of 0.25 could only be used if a second CPE element replacing the parallel capacitance in the Randles circuit was included in the model. This model could only be fitted to the data if the value of this coefficient was approximately 0.83. This reflects the complexity of the multilayered electrode structure, which makes it difficult to model the diffusional component of the low-frequency impedance. This problem, however, does not affect the high-frequency component to the impedance, i.e., that which does not involve a constant phase element related to the electron-transfer reaction contribution. This is an approximation to a complex diffusional geometry coupled to electron transfer.

6. Discussion

6.1. Mass Transfer and Electrode Blocking Effects. The attachment of diisocyanide to gold does not lead to a well-ordered self-assembled monolayer (SAM) as is the case with alkane thiols. For the latter, almost pore-free layers can be prepared and tunneling through them studied. The results shown in Figure 2 indicate that full coverage is not achieved when a DICO film is attached to the Au surface. Figure 12 shows a comparison of the peak current densities for bare Au and for Au | DICO electrodes. For the latter, the peak current, j_p, changes little with sweep rate. The behavior observed is characteristic of a partially blocked surface, equivalent to an array of microelectrodes as discussed by Amatore et al.[26] and Girault et al.[27] Since no information is available on the number of defects present in the film, it is not possible to calculate a value of $k^{0\prime}$ with any confidence from the cyclic voltammetry experiments for DICO-terminated surfaces using a transient technique. If during the time scale of the electrochemical measurement the spherical diffusional fields around the defects do not overlap, the observed behavior is that of an array of microelectrodes and a sigmoidal current−potential relationship is observed. For sufficiently large overlap, linear diffusional conditions are established.[27] Thus, the results obtained from cyclic voltammetry measurements for isocyanide-terminated films will be dependent on the sweep rate employed. In contrast, when the surface is terminated with Pt nanoparticles the response corresponds to a quasi-reversible reaction. The rate constants measured with the different techniques will be analyzed further on.

The use of a steady-state technique, such as the RDE, provides a method for the measurement of $k^{0\prime}$, which is less dependent on the experimental mass transfer conditions, provided the thickness of the diffusional layer is greater than the size of the defects. It is proposed that this was the case for the electrodes investigated in the present work. However, the rate constants measured do include a component related to the number of active sites where the electron-transfer reaction takes place and to the size of these domains.[26,28]

The Pt-terminated surfaces do not display the microheterogeneity of the isocyanide-terminated surfaces, and the diffusional geometry corresponds to linear conditions. The rate constants calculated in this case were always lower than those for a free metal surface (Table 2). Two electron-transfer mechanisms across self-assembled monolayers can be considered: electron hopping and extensive coalescence of particles. Electron hopping between nanoparticles is fast, in particular, considering the overlap of energy levels in the film, and large electrical conductivity has been observed in these materials.[5d−f,29,30] The

partial coalescence of chemically attached nanoparticles within the film resulting in direct contact across the nanoparticulate network is very unlikely since optical spectroscopy clearly indicates that the metal cores retain their integrity within the film.[5g,h] Indeed, Coulombic effects in films have been recently reported by Murray and co-workers,[31] showing not only the presence of intact core−shell particles within the nanostructured films, but also the importance of electron hopping as a conduction mechanism. It should be stressed, however, that these films are inhomogeneous and the rate constants measured correspond to average values.

The diffusional currents for a partially blocked rotating disk electrode have been extensively analyzed by Landsberg et al.[28] The parameters determining behavior are the number density of active areas and their radii. The surface is modeled as an hexagonal array of active sites of radius r_1 and number density N. The diffusional field is confined by a hypothetical cylinder placed between the active sites and the boundary of the diffusion layer of thickness δ. The radius of these cylinders, r_2, is determined by N considering that $N\pi r_2^2 = 1$,[28] and this simple model assumes a value of r_2 such that the total diffusional field is divided into totally confined sections. For $\delta > r_2$, this model leads to an equivalent to the Koutecky−Levich equation given by

$$j^{-1} = j_D{}^{-1} + \frac{|\sum A_n|}{nFDc^b} \tag{14}$$

where j_D is the limiting diffusion current given by

$$j_D = 0.620nFD^{2/3}\nu^{-1/6}c^b\omega^{1/2} \tag{15}$$

and $|\Sigma A_n|$ is a term that takes into account the flux inhomogeneities due to the divergence of the diffusional field close to the partially blocked electrode surface. A test of partial surface blocking is to calculate the intercept of the K.−L. plot at the extreme of polarization, when the reaction is controlled by diffusion. This should extrapolate to zero for an unblocked surface, and to $|\Sigma A_n|/FDc^b$ for a partially blocked electrode.[28,32] The inset in Figure 7 shows a typical example of the behavior of the Pt nanoparticle terminated film electrodes investigated. A limiting value of $j_D{}^{-1}$ of 180 A^{-1} cm^2 was obtained, from which $|\Sigma A_n| = 1.17 \times 10^{-4}$ cm. This value can now be related to the known size of the nanoparticles employed, the average diameter of which was 2.4 nm. If it is considered first that the particles in the film are electrically insulated from each other, $r_1 = 1.2$ nm. Landsberg et al. reported values of the function $f(r_1/r_2) = |\Sigma A_n|/r_2$ calculated as a function of r_1/r_2.[28c] An estimate of r_2 corresponding to the results shown in Figure 7 was carried out by finding the value of r_2 that complied with the condition

$$r_2 = \frac{|\sum A_n|}{f(r_1/r_2)} \tag{16}$$

where $|\Sigma A_n|$ was calculated from the intercept of the K.−L. plot when $\omega \rightarrow \infty$. This procedure led to a value of $r_2 = 50$ nm for $r_1 = 1.2$ nm. This is a surprising result since it implies that the blocking factor[28c] $\phi = 1 - r_1^2/r_2^2$ is 0.9994, i.e., only 0.06% of the surface would be electroactive, in total disagreement with the observed diffusional currents from the RDE experiments. Thus, the value of r_1 employed in the above calculation cannot be correct although previous work with gold nanostructured surfaces of similar structure as used in the present work showed that the particles retained their integrity in the films.[5f−h] It is proposed that in the present case, the basic requirement for applying Landsberg's treatment, i.e., independent isolated centers, is not fulfilled. The porous nature of the film could result in an additional decrease in the value of the rate constant if the material under the top layer were insulating.[32] This is not the case for the present system since good electronic coupling between nanoparticles is apparent in this type of arrays, even in the presence of organic linkers[5d,f] due to the very fast electron-transfer rates resulting from electron hopping.[33]

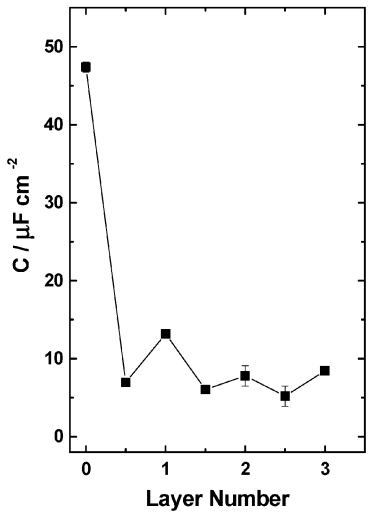

Figure 13. Dependence of the base electrolyte double layer capacitance on the number of layers of diisocyanide and Pt nanoparticles.

The behavior of the nanostructured electrodes indicates the presence of domains where electron transfer takes place that have dimensions much greater than those corresponding to the individual nanoparticles. The lower value of the diffusional currents observed for the nanostructured electrode, however, is a measure of the fraction of effective collisions with centers where electron transfer can take place. For example, for an Au | DICO | Pt electrode (Figure 4), the effective area is 92% that of an unblocked electrode whereas for an Au | DICO | Pt | DICO | Pt |DICO| Pt surface, this value decreases to 65%. The reason for the large decrease in effective area is the higher degree of disorder that accompanies the attachment of successive layers.

6.2. The Interfacial Capacitance. A comparison of the interfacial capacitance between DICO and Pt terminated surfaces in the absence of a redox couple in the solution provides additional information on interfacial structure. The capacitance was obtained by fitting the ac impedance data obtained in the absence of the redox couple. Figure 13 shows the results obtained at the formal potential for the different electrode surfaces studied. It is noteworthy that the capacitance increases on attachment of the metal nanoparticles and decreases when the film is terminated with DICO. The interface can be regarded as an array of capacitors in parallel (see schematic diagram in Figure 14), and therefore the total capacitance, C_T, is given by[34]

$$C_T = \theta C_{Pt} + (1 - \theta)C_{DICO} \tag{17}$$

where θ is the fraction of the surface covered by Pt nanoparticles and C_{Pt} and C_{DICO} are the capacitances of a bare Pt and a DICO-terminated surface. From eq 17, the coverage is given by

$$\theta = \frac{C_T - C_{DICO}}{C_{Pt} - C_{DICO}} \tag{18}$$

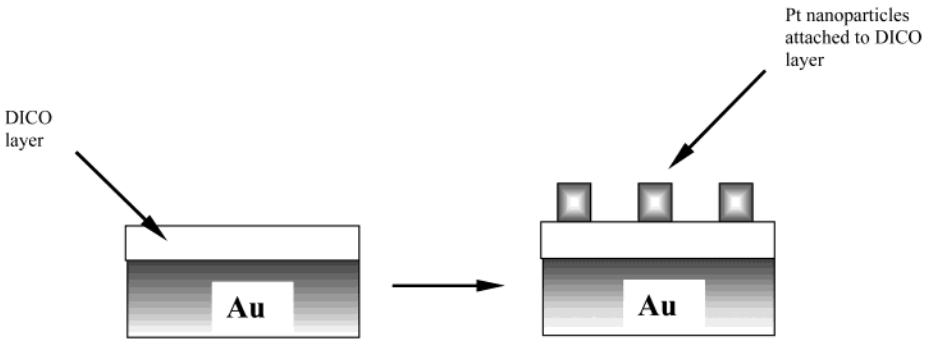

Figure 14. Schematic diagram showing the structures used to estimate coverage of Pt nanoparticles on the nanostructured surface. This diagram is an oversimplification and does not show the imperfections in the DICO layer. The quantities derived from such models represent average properties and are useful for visualizing the contributions of possible structures to the interfacial capacitance.

If the nanoparticles were electronically isolated from the substrate, the contribution C_{Pt} that has to be considered is the series combination of the interfacial capacity of the Pt/solution interface and that of the DICO layer. Therefore, the contribution of the film regions having Pt attached to them would be *less* than that of the DICO film and C_T should, in this case, decrease on attachment of the nanoparticles. This is contrary to experimental observation, and therefore the Pt nanoparticle contribution must be larger than that of DICO. As discussed above, the electron-transfer experiments indicate strong electronic coupling between the metal substrate and the nanoparticles, and between successive layers of particles. This would result in a bypass of the dielectric media constituting the intermediate DICO ligand layers.

The capacitance measured for a bare Pt electrode gave $C_{Pt} = 31\ \mu F\ cm^{-2}$, and taking $C_{DICO} = 6.9\ \mu F\ cm^{-2}$ from the monolayer-covered Au electrode results, the area coverage calculated from eq 18 is approximately 0.25 for the first layer of nanoparticles. This result is at variance with the observed limiting currents for the RDE, which indicate higher coverages. The failure of this simple model to account quantitatively for the observed changes in capacitance is most likely due to the inadequacy of transposing macroscopic capacitance interfacial models to systems where the characteristic dimensions of their constituents are in the nanometer range. However, the capacitance trends shown in Figure 13 give further evidence for electronic communication within the film.

6.3. Comparison of Rate Constants Obtained from Different Techniques. For the ac impedance results, the Randles equivalent circuit is an oversimplification. Although a much more complicated equivalent circuit could have been employed, perhaps allowing for the possibility of more than one electron-transfer mechanism or for transport across the uncovered DICO molecules as well as to the Pt particles, it is much more difficult to model the data reliably when a large number of parameters is employed. The rate constants obtained using the Randles circuit were reasonably comparable with those obtained using the rotating disk electrode. One difficulty with the analysis for Pt-terminated films is that at least two processes in series should be considered, i.e., tunneling from the metal to nanoparticles and from the particles to the redox species in solution. In what follows, it is considered that the hopping exchange rate within the film is much faster than the interfacial rate of electron transfer, and only one activation barrier needs to be considered. Therefore, the values of $k^{0'}$ measured are only related to interfacial electron transfer.

There is a considerable scatter in the rate constants calculated (Tables 1−3). The results from CV and RDE experiments for Pt-terminated surfaces agree with each other within a factor of 2 for $\alpha = 0.5$, and this is probably a consequence of the similarity of the average surface properties being probed by these techniques. In contrast, ac impedance probes within the inhomogenities of the surface as demonstrated by the observation of behavior akin to a porous structure. Cyclic voltammetry is equivalent to a low-frequency measurement, and hence it is not surprising that CV and RDE methods give similar results. In contrast, ac impedance would be more sensitive to the details of the structure of the film and to imperfections in the isocyanide layers.

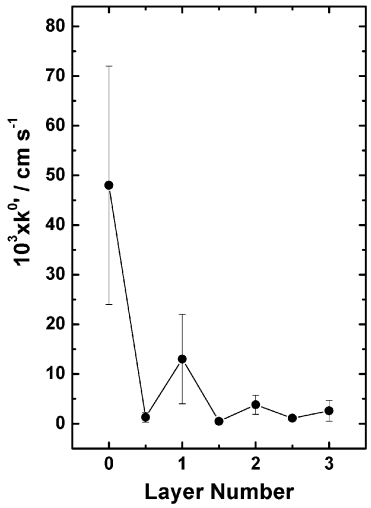

Figure 15. Variation of the formal rate constant $k^{0'}$ with the number of layers of diisocyanide and Pt nanoparticles.

6.4. The Values of $k^{0'}$. Figure 15 summarizes the average values of the rate constant for the different films investigated. The standard deviation of results obtained with the different techniques is also indicated in this Figure. Despite the dispersion of results, a clear trend is in evidence and it is noteworthy that the rate constants are always higher when the film is terminated with Pt compared with the results for DICO-terminated films. A similar behavior has been previously observed for these types of films when dithiols are used as tethers.[5a]

There are three possible reasons for this effect, related to the number density of metal centers on which electron transfer takes place, to the density of states within the nanoparticles, and/or to electron hopping between nanoparticles through the film. It is very unlikely that the rate of electron hopping across the nanostructured film is responsible for the oscillations in $k^{0'}$ shown in Figure 15 for the different terminations. Murray et al.[31] used a simple electron hopping model to discuss electron transfer through nanostructured films and for particles with a center-to-center separation of 5.14 nm, the rate constant for

electron hopping, k_{HOP}, was $(2 \pm 1) \times 10^6$ s^{-1}. This separation corresponded to 22 methylene groups separating the nanoparticles. Taking an estimated electronic coupling factor $\beta \approx 8$ nm^{-1}, a value of $k_{HOP} \approx 10^{12}$ s^{-1} can be estimated for the particles within the Pt−isocyanide film. This very large number indicates only that electron hopping cannot be rate determining.

It is difficult to separate the other two possible contributions to the rate constant, the density of states and the particle number density. For gold, quantum size effects become apparent only when the diameter of the metal core is less than 1.4 nm, for which the observation of d−d transitions becomes possible.[35] Also, it is only this size range for which nanoparticles start to exhibit redox chemical character and a band gap.[8a,b] The size of the metal clusters studied in the present work is greater than that required to observe these effects, and therefore the most likely reason for the results shown in Figure 15 is a decrease in the number density of the centers where electron transfer can take place, compared with the bulk metal.

The rate constants calculated for bare gold are at the measuring limit of the techniques employed. The hexacyanoferrate(II)/(III) couple has been extensively investigated previously, and the rate constants reported appear to be dependent on both the electrode material used and its pretreatment. Values of 0.019 cm s^{-1} in 0.5 M $NaClO_4$ [36a] (for Au(111)), 0.035 cm s^{-1} in 0.5 M Li_2SO_4,[36b] and 0.01, 0.06 and 0.1 cm s^{-1} for 1 M $LiNO_3$, $NaClO_4$, and KF, respectively[36c] (for polycrystalline Au) have been reported. For the latter, a strong dependence of k^0 on the nature and concentration of the cation in the base electrolyte was found. A similar spread of results has been reported for Pt. For example, values of the rate constant of 0.13 and 0.09 cm s^{-1} for 0.5 M K_2SO_4 and 1 M KCl, respectively,[37] and 0.067 cm s^{-1} in 0.5 M K_2SO_4 [21] have been measured.

The irreproducibility of the rate constant might be a consequence of adventitious decomposition of the hexacyanoferrate on the electrode surface. The presence of cyanide-containing groups on Pt has been detected by Kitamura et al.[38] and by Stieble and Jüttner.[24] By contrast, Christensen et al.[39] did not find evidence of adsorbed cyano-containing species. A comprehensive spectroscopic study by Pharr and Griffiths[40] demonstrated, however, the importance of control of the electrode potential for the formation of adsorbed layers of products that can affect the Pt surface reactivity. In particular, a necessary condition for the detection of irreversibly adsorbed species was that the anodic potential excursion had to be more positive than 0.8 V vs SCE. FTIR spectroscopy demonstrated that electrodes cycled to a less positive limit did not show evidence of film formation, but decomposition became evident after 1 h of cycling between −0.33 and +0.8 V. The anodic limit in the experiments described in the present work was +0.45 V, and therefore no decomposition and film formation was expected to take place on the nanostructured electrodes investigated.

The spread in experimental values for $k^{0\prime}$ for the nanostructured film is therefore not related to the decomposition of hexacyanoferrate but most likely to the inhomogeneity of the layers from different preparations. The diversity in rate constant values measured for the hexacyanoferrate couple clearly shows that the conditions of the measurements determine, to some extent, the values obtained. However, a comparison of results obtained with similar conditions, as described in the present work, provides an insight into the kinetics of electron-transfer reaction at nanostructured electrodes and demonstrates that kinetics is determined by the electron-transfer reaction at the nanoparticle/solution interface.

7. Conclusions

It has been shown that it is possible to create nanostructured surfaces using diisocyanide ligands as molecular tethers. The advantage of the use of isocyanides lies in their versatility in binding to a wide range of transition metals. The electrochemical properties of the multilayers synthesized was strongly dependent on the surface termination employed: when the surface was terminated with Pt nanoparticles, fast electron transfer to aqueous redox couples took place, but if the surface was terminated with diisocyanide, inhibition of electron transfer was observed. The decrease in the rate constants is less than an order of magnitude for the hexacyanoferrate(II)/(III) couple for three DICO | Pt layers, indicating that transport between nanoparticles within the film is not inhibited by the presence of a long-chain hydrocarbon residue. The electron transport mechanism proposed is similar to that previously discussed by Murray et al.,[31,33] much like that observed for electron transport between redox centers in polymers.

The interest of the present work is two-fold: (1) it shows that nanostructures can be prepared using bifunctional ligands other than dithiols and (2) the use of electrocatalytic metals to construct the nanomaterial opens up interesting perspectives for the study of size effects in electrocatalysis.

Acknowledgment. The support of the Wolfson Foundation (S.L.H.) is acknowledged. Useful discussions with Prof. E. Ahlberg, Göteborg University, on electron-transfer reactions at partially blocked electrodes, are also gratefully acknowledged.

References and Notes

(1) (a) Kinoshita, K. *J. Electrochem. Soc.* **1990**, *137*, 845. (b) Takasu, Y.; Fujii, Y.; Yasuda, K.; Iwanaga, I.; Matsuda, Y. *Electrochim. Acta* **1989**, *34*, 453. (c) Takasu, Y.; Ohashis, N.; Zhang, X. G.; Murakami, Y.; Minagawa, H.; Sato, S.; Yahikozawa, K. *Electrochim. Acta* **1996**, *41*, 2595. (d) Friedrich, K. A.; Henglein, F.; Stimming, U.; Unkauf, W. *Electrochim. Acta* **2000**, *45*, 3283.

(2) (a) Hurata, M. *Catal. Today* **1997**, *36*, 153. (b) Haruta, M.; Yamada, N.; Kobayashi, T.; Iijima, S. *J. Catal.* **1989**, *115*, 301.

(3) (a) Maye, M. M.; Lou, Y.; Zhong, C.-J. *Langmuir* **2000**, *16*, 7520. (b) Zhong, C.-J.; Maye, M. M. *Adv. Mater.* **2001**, *13*, 1507. (c) Lou, Y.; Maye, M. M.; Han, L.; Luo, J.; Zhong, C.-J. *J. Chem. Soc., Chem. Commun.* **2001**, 473.

(4) (a) Whetten, R. L.; Shafigullin, M. N.; Khoury, J. T.; Schaaf, T. G.; Vezmar, I.; Alvarez, M. M.; Wilkinson, A. *Acc. Chem. Res.* **1999**, *32*, 397. (b) Templeton, A. C.; Wuelfing, W. P.; Murray, R. W. *Acc. Chem. Res.* **2000**, *33*, 27. (c) Brust, M.; Kiely C. J. *Colloids Surf. A* **2002**, *202*, 175. (d) Schiffrin, D. J. *MRS Bull.* **2001**, *26*, 1015.

(5) (a) Bethell, D.; Brust, M.; Schiffrin, D. J.; Kiely, C. J. *J. Electroanal. Chem.* **1996**, *409*, 137. (b) Yamada, M.; Nishihara, H. *J. Chem. Soc., Chem. Commun.* **2002**, 2578. (c) Lu, M.; Li, H.; Yu, B. Z.; Li, H. L. *J. Colloid Interface Sci.* **2002**, *248*, 376. (d) Musick, M. D.; Keating, C. D.; Keefe, M. H.; Natan, M. J. *Chem. Mater.* **1997**, *9*, 1499. (e) Grabar, K. C.; Freeman, R. G.; Hommer, M. B.; Natan, M. J. *Anal. Chem.* **1995**, *67*, 735. (f) Baum, T.; Bethell, D.; Brust, M.; Schiffrin, D. J. *Langmuir* **1999**, *15*, 866. (g) Gittins, D. I.; Bethell, D.; Nichols, R. J.; Schiffrin, D. J. *Adv. Mater.* **1999**, *11*, 737. (h) Gittins, D. I.; Bethell, D.; Nichols, R. J.; Schiffrin, D. J. *J. Mater. Chem.* **2000**, *10*, 79.

(6) (a) Chen, S.; Murray, R. W. *J. Phys. Chem. B* **1999**, *103*, 9996. (b) Wuelfing, W. P.; Zamborini, F. P.; Templeton, A. C.; Wen, X.; Yoon, H.; Murray, R. W. *Chem. Mater.* **2001**, *13*, 87. (c) Templeton, A. C.; Zamborini, F. P.; Wuelfing, W. P.; Murray, R. W. *Langmuir* **2000**, *16*, 6682. (d) Zamborini, F. P.; Hicks, J. F.; Murray, R. W. *J. Am. Chem. Soc.* **2000**, *122*, 4514. (e) Wuelfing, W. P.; Green, S. J.; Pietron, J. J.; Cliffel, D. E.; Murray, R. W.; *J. Am. Chem. Soc.* **2000**, *122*, 11465.

(7) (a) Park, S.; Weaver, M. J. *J. Phys. Chem. B* **2002**, *106*, 8667. (b) Park, S.; Tong, Y. Y.; Wieckowski, A.; Weaver, M. J. *Electrochem. Commun.* **2001**, *3*, 509.

(8) (a) Ingram, R. S.; Hostetler, M. J.; Murray, R. W.; Schaaf, T. G.; Khoury, J. T.; Whetten, R. L.; Bigioni, T. P.; Guthrie, D. L.; First, P. N. *J. Am. Chem. Soc.* **1997**, *119*, 9279. (b) Chen, S.; Ingram, R. S.; Hostetler, M. J.; Pietron, J. J.; Murray, R. W.; Schaaf, T. G.; Khoury, J. T.; Alvarez, M. M.; Whetten, R. L. *Science* **1998**, *280*, 2098−2101. (c) Chen, S. *J. Phys. Chem. B* **2000**, *104*, 663. (d) Pietron, J. J.; Hicks, J. F.; Murray, R. W. *J. Am. Chem. Soc.* **1999**, *121*, 5565. (e) Chen, S.; Murray, R. W.; Feldberg, S. W. *J. Phys. Chem. B* **1998**, *102*, 9898.

(9) (a) Horswell, S. L.; Kiely, C. J.; O'Neil, I. A.; Schiffrin, D. J. *J. Am. Chem. Soc.* **1999**, *121*, 5573. (b) Horswell, S. L.; O'Neil, I. A.; Schiffrin, D. J. *J. Phys. Chem. B* **2001**, *105*, 941.

(10) (a) Rampino, L. D.; Nord, F. F. *J. Am. Chem. Soc.* **1942**, *63*, 2745. (b) Henglein, A.; Ershov, B. G.; Malow, M. *J. Phys. Chem.* **1995**, *99*, 14129. (c) Matheson, M. S.; Lee, P. C.; Meisel, D.; Pelizzetti, E. *J. Phys. Chem.* **1983**, *87*, 394. (d) Leheny, A. R.; Rossetti, R.; Brus, L. E. *J. Phys. Chem.* **1985**, *89*, 211. (e) Chen, D.-H.; Yeh, J.-J.; Huang, T.-C. *J. Colloid Interface Sci.* **1999**, *215*, 159. (f) Henglein, A.; Giersig, M. *J. Phys. Chem. B* **2000**, *104*, 6767. (g) Petroski, J. M.; Green, T. C.; El-Sayed, M. A. *J. Phys. Chem. A* **2001**, *105*, 5542.

(11) (a) Ahmadi, T. S.; Wang, Z. L.; Henglein, A., El-Sayed, M. A. *Chem. Mater.* **1996**, *8*, 1161. (b) Teranishi, T.; Kurita, R.; Miyake, M. *J. Inorg. Organomet. Polym.* **2000**, *10*, 145. (c) Ahmadi, T. S.; Wang, Z. L.; Green, T. C.; Henglein, A.; El-Sayed, M. A. *Science* **1996**, *272*, 1924. (d) Petroski, J. M.; Wang, Z. L.; Grenn, T. C.; El-Sayed, M. A. *J. Phys. Chem. B* **1998**, *102*, 3316.

(12) Reetz, M. T.; Quaiser, S. A. *Angew. Chem., Intl. Ed. Engl.* **1995**, *34*, 2240.

(13) (a) Yee, C.; Scotti, M.; Ulman, A.; White, H.; Rafailovich, M.; Solokov, J. *Langmuir* **1999**, *15*, 4314. (b) Perez, H.; Pradeau, J.-P.; Albouy, P.-A.; Perez-Omil, J. *Chem. Mater.* **1999**, *11*, 3460. (c) Sarathy, K. V.; Raina, G.; Yadav, R. T.; Kulkami, G. U.; Rao, C. N. R. *J. Phys. Chem. B* **1997**, *101*, 9876.

(14) (a) Miyazaki A.; Nakano, Y. *Langmuir* **2000**, *16*, 7109. (b) Sastry, M.; Patil, V.; Mayya, K. S.; Paranjape, D. V.; Singh, P.; Sainkar, S. R. *Thin Solid Films* **1998**, *324*, 239. (c) Hirai, H. *J. Macromol. Sci.-Chem.* **1979**, *A13*, 633. (d) Hirai, H.; Nakao, Y.; Toshima, N. *J. Macromol. Sci.-Chem.* **1979**, *A13*, 727. (e) Mizukoshi, Y.; Oshima, R.; Maeda, Y.; Nagata, Y. *Langmuir* **1999**, *15*, 2733.

(15) (a) Meguro, K.; Torizuka, M.; Esumi, E. *Bull. Chem. Soc. Jpn.* **1988**, *61*, 341. (b) Bönnemann, H.; Brijoux, W.; Brinkmann, R.; Dinjus, E.; Joussen, T.; Korall, B. *Angew. Chem., Intl. Ed. Engl.* **1995**, *34*, 2240.

(16) Henderson, J.; Feng, S.; Ferrence, G.; Bein, T.; Kubiak, C. *Inorg. Chim. Acta* **1996**, *242*, 115.

(17) (a) Solla-Gullón, J.; Montiel, V.; Aldaz, A.; Clavilier, J. *J. Electroanal. Chem.* **2000**, *491*, 69. (b) Solla-Gullón, J.; Montiel, V.; Aldaz, A.; Clavilier, J. *Electrochem. Commun.* **2002**, *4*, 716.

(18) Z-view and Z-plot software, Solartron Instruments, UK.

(19) Bard, A. J.; Faulkner, L. R. *Electrochemical Methods: Fundamentals and Applications*; Wiley: New York, 1985.

(20) Nicholson, R. S. *Anal. Chem.* **1965**, *37*, 1351.

(21) Jahn, D.; Vielstich, W. *J. Electrochem. Soc.* **1962**, *109*, 1849.

(22) de Levie, R. *Adv. Electrochem. Electrochem. Eng.* **1976**, *21*, 539.

(23) (a) Müller, L.; Dietzsch, S. *Z. Phys. Chem., Leipzig* **1984**, *265*, 212. (b) Frumkin, A. N.; Petry, O. A.; Nikolaeva-Fedorovich, N. V. *Electrochim. Acta* **1963**, *8*, 177.

(24) (a) Stieble, M.; Jüttner, E. *J. Electroanal. Chem.* **1990**, *290*, 163−180. (b) Winkler, K. *J. Electroanal. Chem.* **1995**, *388*, 151. (c) Kawiak, J.; Jędral, T.; Galus, Z. *J. Electroanal. Chem.* **1983**, *145*, 163. (d) Beriet, C.; Pletcher, D. *J. Electroanal. Chem.* **1993**, *361*, 93.

(25) (a) Tammeveski, K.; Kontturi, K.; Nichols, R. J.; Potter, R. J.; Schiffrin, D. J. *J. Electroanal. Chem.* **2001**, *515*, 101. (b) Sarapuu, A.; Vaik, K.; Schiffrin, D. J.; Tammeveski, K. *J. Electroanal. Chem.*, in press.

(26) Amatore, C.; Savéant, J. M.; Tessier, D. *J. Electroanal. Chem.* **1983**, *147*, 39.

(27) Lee, H. J.; Beriet, C.; Ferrigno, R.; Girault, H. H. *J. Electroanal. Chem.* **2001**, *502*, 138.

(28) (a) Landsberg, R.; Thiele, R. *Electrochim. Acta* **1966**, *11*, 1243. (b) Scheller, F.; Landsberg, R.; Müller, S. *J. Electroanal. Chem.* **1969**, *20*, 375. (c) Scheller, F.; Müller, S.; Landsberg, R.; Spitzer, J.-J. *J. Electroanal. Chem.* **1968**, *19*, 187. (d) Lindemann, J.; Landsberg, R. *J. Electroanal. Chem.* **1971**, *29*, 261.

(29) Brust, M.; Bethell, D.; Schiffrin, D. J.; Kiely, C. J. *Adv. Mater.* **1995**, *7*, 795.

(30) Terril, R. H.; Postlethwaite, T. A.; Chen, C.-H.; Poon, C.-D.; Terzis, A.; Chen, A.; Hutchison, J. E.; Clark, M. R.; Wignall, G.; Londono, J. D.; Superfine, R.; Falvo, M.; Johnson, C. S., Jr.; Samulski, E. T.; Murray, R. W. *J. Am. Chem. Soc.* **1995**, *117*, 12537.

(31) Hicks, J. F.; Zamborini, F. P.; Osisek A. J.; Murray, R. W. *J. Am. Chem. Soc.* **2001**, *123*, 7048−53.

(32) Ahlberg, E.; Falkenberg, F.; Manzanares, J.; Schiffrin, D. J. *J. Electroanal. Chem.*, submitted.

(33) Wuelfing, W. P.; Murray, R. J. *J. Phys. Chem. B* **2002**, *106*, 3139.

(34) (a) Parsons, R. *J. Electroanal. Chem.* **1964**, *7*, 136. (b) Frumkin, A. N.; Damaskin, B. B. In *Modern Aspects of Electrochemistry*; Bockris, J. O'M., Ed.; Butterworths: London, 1964; Vol. 3, p 149.

(35) Schaaf, T. G.; Shafigullin, M. N.; Khoury, J. T.; Vezmar, I.; Whetten, R. L.; Cullen, W. G.; First, P. N.; Gutiérrez-Wing, C.; Ascensio, J.; José-Yacamán, M. J. *J. Phys. Chem. B* **1997**, *101*, 7885.

(36) (a) Janek, R. P.; Fawcett, W. R.; Ulman, A. *Langmuir* **1998**, *14*, 3011. (b) Geblewicz, G.; Schiffrin, D. J. *J. Electroanal. Chem.* **1988**, *244*, 27. (c) Peter, L. M.; Dürr, W.; Bindra, P.; Gerischer, H. *J. Electroanal. Chem.* **1976**, *71*, 31.

(37) Randles, J. E. B.; Somerton, K. W. *Trans. Faraday Soc.* **1952**, *48*, 937.

(38) Kitamura, F.; Nanbu, N.; Ohsaka, T.; Tokuda, K. *J. Electroanal. Chem.* **1998**, *456*, 113.

(39) Christensen, P.; Hamnett, A.; Trevellick, P. *J. Electroanal. Chem.* **1988**, *242*, 23.

(40) (a) Pharr, C. M.; Griffiths, P. R. *Anal. Chem.* **1997**, *69*, 4665. (b) Pharr, C. M.; Griffiths, P. R. *Anal. Chem.* **1997**, *69*, 4673.